ACS OMEGA

Open Access

http://pubs.acs.org/journal/acsodf

Article

ReaxFF-Based Molecular Dynamics Study of the Mechanism of the Reaction of N_2O_4 with H_2O

Yi Guo, Gan Tian, Xinlong Chang,* Zhanmei Tang, Zhiyong Huang, Dejun Liu, and Xinzhi Yang

Cite This: *ACS Omega* 2024, 9, 18893−18900

Read Online

ACCESS | Metrics & More | Article Recommendations

ABSTRACT: During long-term storage of the liquid propellant N_2O_4, it absorbs H_2O to form the $N_2O_4(H_2O)_n$ system, and this in turn generates HNO_3, HNO_2, and other substances in the storage tank because of corrosion, which seriously affects the performance of weaponry. In this work, we carried out computational simulations of N_2O_4 with different masses of water based on ReaxFF, analyzed the reaction intermediates and products, and investigated the mechanism of the reaction of N_2O_4 with H_2O and of $N_2O_4(H_2O)_n$. The results show that the reaction product $\omega(HNO_3+HNO_2)$ undergoes a rapid growth in the early stage of the reaction and then tends toward dynamic equilibrium; the potential energy of the system decreases with the increase of $\omega(H_2O)$, the reaction rate increases, and the rate of decomposition of HNO_2 to form HNO_3 increases. When $\omega(H_2O)$ is 0.2 or 1.0%, the intermediate products are $N_2O_4H_2O$ or $N_2O_4(H_2O)_2$, respectively, and the reaction proceeds along two paths; when $\omega(H_2O) \geq 2.0\%$, $N_2O_4(H_2O)_3$ appears as the intermediate product, HNO_3 and HNO_2 are directly produced in one step, and a stable current loop can be formed within the whole system.

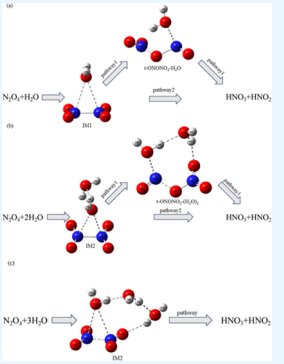

1. INTRODUCTION

N_2O_4 is often used as an oxidizer in two-component liquid propulsion systems in the first and second stages of launch vehicles, owing to its high density, high specific impulse, and strong oxidizing properties.[1] In the case of long-term storage, N_2O_4 absorbs H_2O from the surrounding environment to form the $N_2O_4(H_2O)_n$ system, which in turn generates HNO_3, HNO_2, and other substances, accelerating the corrosion of the storage tank and causing structural damages and propellant leakage, which are hazardous and threaten the safety of the equipment.[2] Therefore, the study of the reaction mechanism of N_2O_4 and H_2O is of great significance for the structural design of weapons and equipment as well as for long-term storage safety.

At present, the test and analysis methods for N_2O_4 are mainly based on the Chinese military standard GJB1673−93; further, owing to the limitation of the instruments, the accuracy of test results is poor, and only parameters such as the equivalent water content of N_2O_4 with a water content of ≤0.4% can be determined, whereas determination of the content of HNO_3, HNO_2, and other substances is impossible. In addition, N_2O_4 is a volatile, reddish-brown transparent liquid at room temperature with strong oxidizing and toxic properties.[3] Therefore, the design and performance of the experiments are challenging.

In principle, quantum chemistry (QC) is applicable to all chemical systems but not to large systems owing to the high computational effort.[4] Although conventional force fields such as MM3,[5,6] DREIDING,[7] and EFF[8] can be applied in the case of large systems, they can only describe the interactions between molecules and those within condensed phase systems. ReaxFF is a bond order-based reaction force field, originally proposed by van Duin in 2001, that has no energy or force discontinuities, even during a reaction.[9] Thus, ReaxFF can describe the formation and dissociation of chemical bonds. The classical treatment of reactive chemistry made available by the ReaxFF method has enabled numerous studies of phenomena occurring on scales that were previously inaccessible via computational methods. In particular, ReaxFF is capable of modeling reaction events involving reactions at the interface between the solid, liquid, and gas phases, which is possible because the ReaxFF description of each element can be transferred across phases. For example, the same system of mathematical forms is used for an oxygen atom, whether that oxygen is in the gas phase as O_2, in the liquid phase within an H_2O molecule, or bound in a solid oxide. This transferability coupled with lower computational costs that allow for longer simulation time scales enables ReaxFF to consider phenomena that depend not only on the reactivity of the species involved but also on dynamic factors such as diffusivity and solubility that affect how species migrate through the system. This allows ReaxFF to model complex processes involving multiple stages in contact with each other.[10] Zhao[11] and Liu[12] et al. simulated

Received: November 5, 2023
Revised: February 17, 2024
Accepted: February 23, 2024
Published: April 15, 2024

the combustion and explosion of N_2O_4 and combustant based on the ReaxFF molecular dynamics simulation method, but the system remains in a state of rapid warming and long-term maintenance of the high temperatures. At present, few studies have focused on the reaction mechanism of N_2O_4 with H_2O, and these were mainly based on the density functional theory (DFT) to explore the isomerization and reaction process.[13−24] Only a limited number of tests have been performed by AFRPL,[25] which is not enough to perfect the reaction path.

In this study, ReaxFF molecular dynamics simulation was used to simulate the intermediates and products of the reaction of N_2O_4 with different mass fractions of H_2O, and combined with the results of the previous work of the group, the reaction course of the $N_2O_4(H_2O)_n$ system was investigated based on DFT, to analyze the reaction mechanism between N_2O_4 and H_2O at room temperature.

2. COMPUTATIONAL METHOD

Molecular dynamics studies of N_2O_4 and H_2O (ω = 0.2−8%) were based on the results of Brown C.T.[25] and the Chinese military standard GJB1673−93. The mixing ratios of N_2O_4 and H_2O are shown in Table 1. The initial configurations of N_2O_4 and H_2O were optimized using Materials Studio software.[26] The initial reactants were randomly inserted into the simulation box, and then, the periodic system was constructed using the amorphous cell module. A conjugate gradient method was adopted for the initial system to perform energy minimization calculations, which facilitate the subsequent relaxation operation. According to the conclusions of Miller,[14] N_2O_4 and H_2O were subjected to 90 ps isothermal isotropic (NVT) kinetic equilibrium with a step size of 0.3 fs at a temperature of 293 K. Temperature control was achieved using the Berendsen method with a temperature damping coefficient of 0.1 ps. Atomic and molecular species and dynamic trajectories were determined every 100 steps. All MD simulations were performed in the Lammps package[27] using the ReaxFF method.[28] In order to verify the reaction products, the polarization curves for a model Al alloy in N_2O_4 with different $\omega(H_2O)$ values were tested. Further, the reaction process of N_2O_4 with different $\omega(H_2O)$ was explored in conjunction with the previous work of the group.[29]

Table 1. Mixing Ratio of N_2O_4 to H_2O

water content/wt %	0.2	0.6	1	2	4	6	8
N_2O_4/n	4900	1600	950	480	235	155	112
H_2O/n	50	50	50	50	50	50	50

3. RESULTS AND DISCUSSION

3.1. Reaction Products HNO_3 and HNO_2. According to the conclusions of Liu,[1,2] the main corrosive intermediates generated by the reaction of N_2O_4 with H_2O are HNO_3 and HNO_2, and their mass fractions depending on the H_2O amount reacting with N_2O_4 are shown in Figure 1. In the initial stage of the reaction, $\omega(HNO_3{+}HNO_2)$ rapidly increases, and then, its mass fraction is gradually stabilized, reaching dynamic equilibrium, with a further increase in the amount of formed products in the system. In order to verify the corrosion intensity of H_2O-containing N_2O_4, a certain type of aluminum alloy was selected to carry out the polarization curve test, the results of which are shown in Figure 2. The electrochemical corrosion current densities obtained from the fitting are listed in Table 2. When $\omega(H_2O)$ < 1.0%, the measured polarization curves were extremely unstable, and no obvious equilibrium electrode potential appeared. As shown in Figure 1, the least amount of HNO_3 + HNO_2 was generated. Since N_2O_4 is not conductive, this also led to an uneven distribution of the generated ions in the solution, which were in a free state and could not form a stable current loop. With the increase in $\omega(H_2O)$, the number of ions generated within the $N_2O_4(H_2O)_n$ system gradually increased, and as shown in Figure 2, $\omega(H_2O)$ = 1.0% is the detection limit using the polarization curve. When $\omega(H_2O)$ > 1.0%, the polarization curve tends to be regular, indicating that a sufficient number of ions exist within the solution to form a stable current loop. Further, when $\omega(H_2O)$ > 2.0%, as shown in Table 2, the corrosion current density changes abruptly, and its corresponding polarization curve is compared to $\omega(H_2O)$ = 2.0%. Further, a significant passivation area and pitting potential E_b of about 0.3 V, combined with the results in Figure 1, indicate that passivation occurs on the surface of the specimen when $\omega(H_2O)$ > 2.0%, while the dissolution film formation equilibrium reaction occurs at a higher corrosion rate.

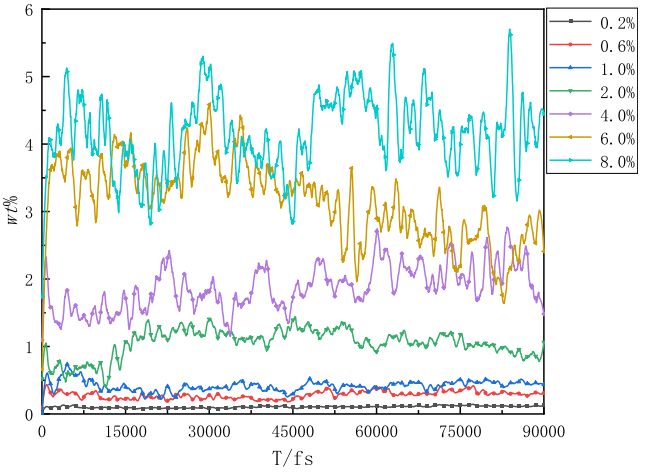

Figure 1. $\omega(HNO_3{+}HNO_2)$ during the reaction of N_2O_4 with different $\omega(H_2O)$.

Based on the results in Figures 1 and 2, the changes in the potential energy (ΔE_p) during the reaction of N_2O_4 with $\omega(H_2O)$ = 0.2, 1.0, 2.0, and 6.0% were analyzed as shown in Figure 3, with the unit au/atom meaning the total potential energy of the system divided by the total number of atoms. When N_2O_4 comes into contact with H_2O, the potential energy of the whole system decreases dramatically, and an exothermic chemical reaction occurs. Subsequently, the generated HNO_2 absorbs heat and undergoes decomposition that leads to a rise in the potential energy of the system; eventually, when the reaction equilibrium is reached in the system, its potential energy also reaches a stable state. Moreover, with the increase in $\omega(H_2O)$, the potential energy of the system decreases, the rate of decrease is the highest in the initial stage, and the final equilibrium state is also lower, which indicates that the reaction rate is faster, and the energy released is also larger.

Figure 4 shows the variation in the amount of HNO_3 and HNO_2 during the course of the reaction between N_2O_4 and different $\omega(H_2O)$. As shown in Figure 4, the production of HNO_2 can be roughly divided into three phases: a period of

https://doi.org/10.1021/acsomega.3c08695
ACS Omega 2024, 9, 18893−18900

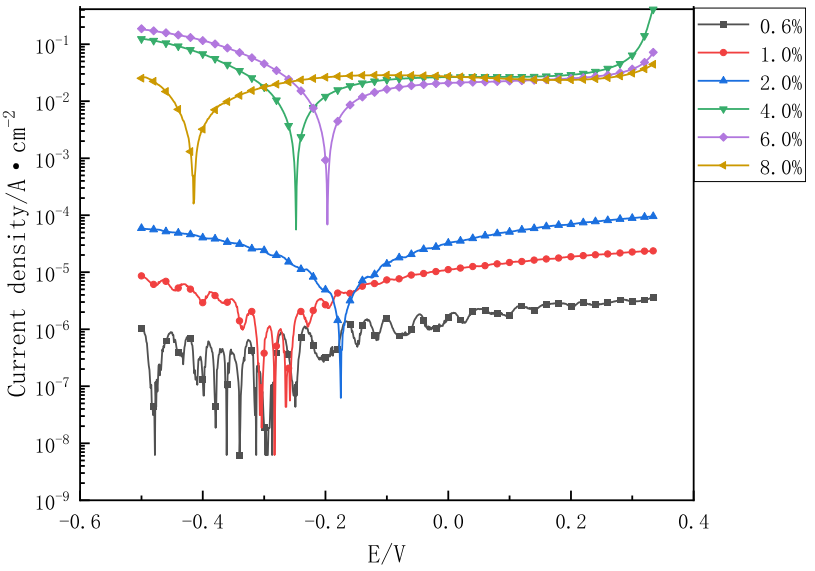

Figure 2. Polarization curves of the type XX aluminum alloy for the reaction of different $\omega(H_2O)$ ions with N_2O_4.

Table 2. Corrosion Current Density of the Type XX Aluminum Alloy for the Reaction of Different $\omega(H_2O)$ with N_2O_4

water content/wt %	0.6	1	2	4	6	8
I_{corr} (A/cm^2)		1.54×10^{-8}	3.50×10^{-8}	4.97×10^{-6}	7.30×10^{-6}	7.06×10^{-5}

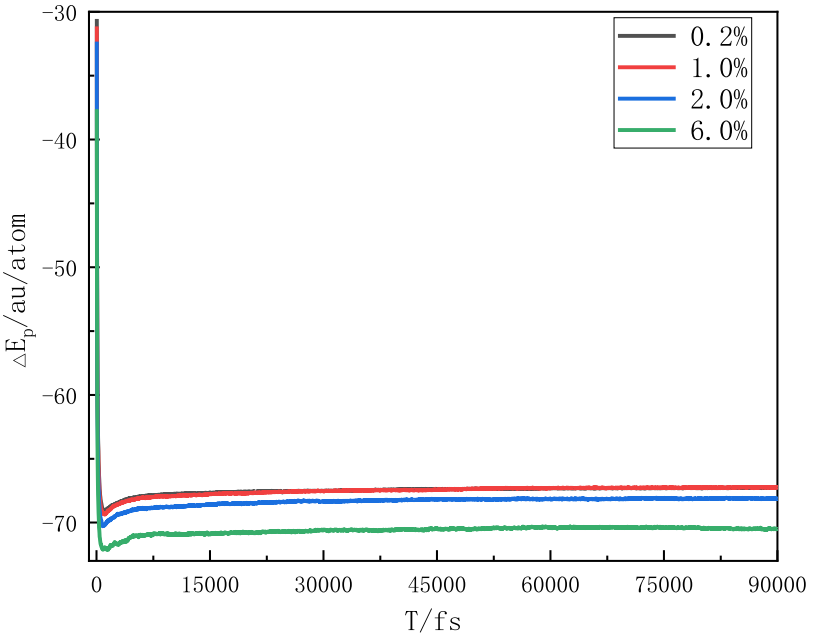

Figure 3. Potential energy changes for the reaction of different amounts of H_2O with N_2O_4.

rapid increase in the amount of HNO_2 produced, a period of slow decrease in the amount of HNO_2 produced, and a stabilization period; on the other hand, the production of HNO_3 has only a period of gradual increase in the amount of HNO_3 produced and a stabilization period. In the early stage of the reaction, the production rate and quantity of HNO_2 are higher than that of HNO_3, but as the reaction proceeds, HNO_2 is further decomposed into HNO_3 and NO: $3HNO_2 \rightarrow HNO_3 + 2NO + H_2O$.

Consistent with the conclusions of AFRPL,[25] when $\omega(H_2O)$ = 0.2%, the amount of HNO_3 and HNO_2 is almost the same after the reaction is stabilized. When $\omega(H_2O)$ is increased, the yield of HNO_2 always remains low because the decomposition of HNO_2 produces H_2O that continues to react with N_2O_4: $N_2O_4 + H_2O \rightarrow HNO_3 + HNO_2$.

Therefore, HNO_2 does not decompose completely, and the whole system remains in a dynamic equilibrium. However, the reaction time required for the amount of HNO_3 to exceed that of HNO_2 continuously reduces. As shown in Figure 3d, the amount of HNO_3 generated exceeds that of HNO_2 at T = 1200 fs, indicating that the reaction rate of the system increases with $\omega(H_2O)$, which is also verified by the results of Multer.[14]

3.2. Intermediate $N_2O_4(H_2O)_n$. The reaction between N_2O_4 and H_2O first produces the $N_2O_4(H_2O)_n$ complex due to

https://doi.org/10.1021/acsomega.3c08695
ACS Omega 2024, 9, 18893−18900

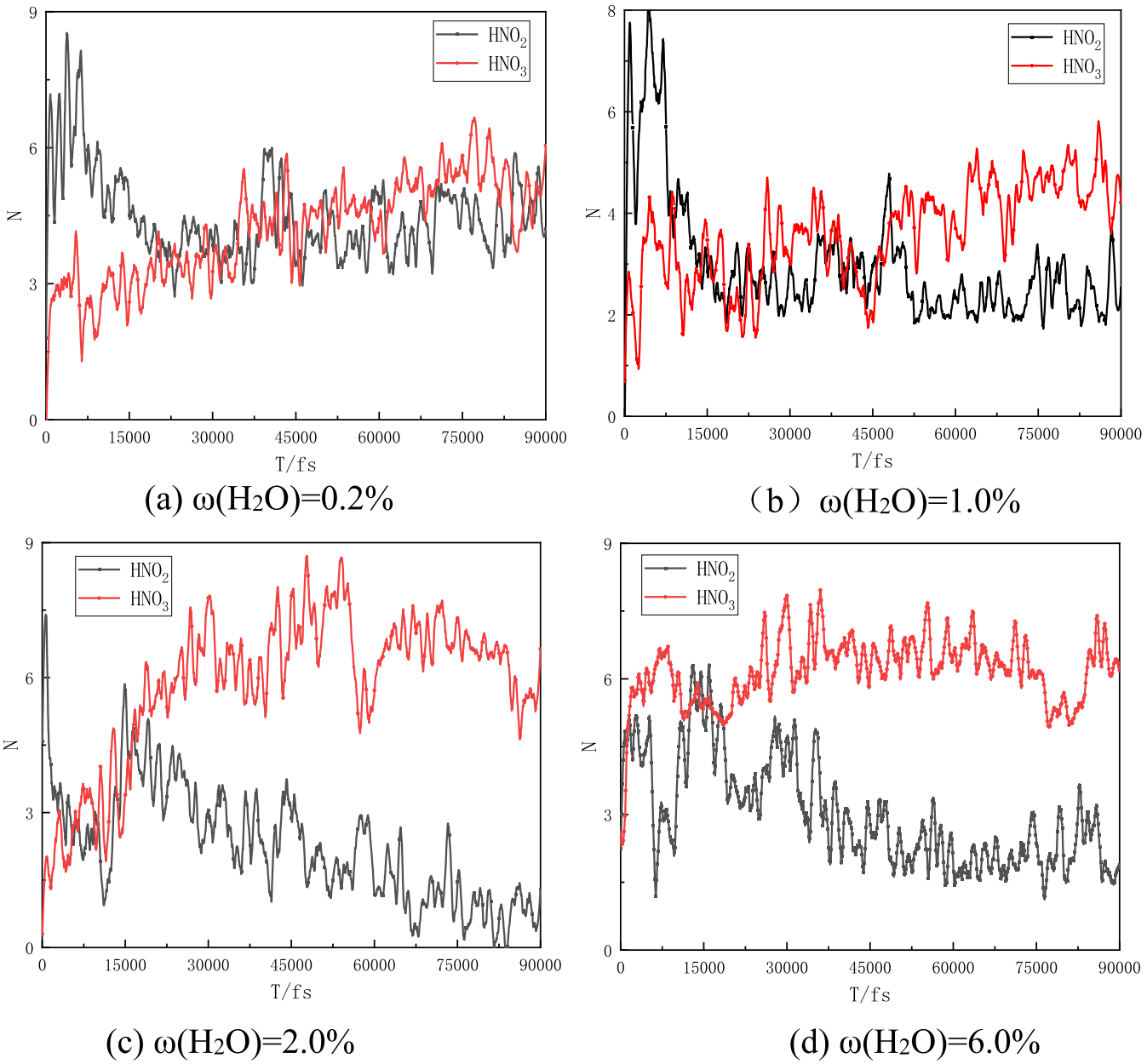

Figure 4. Variation in amount of HNO_3 and HNO_2 during the course of the reaction of N_2O_4 with different $\omega(H_2O)$.

hydrogen bonding,[14] which further affects the course of the reaction depending on the value of n.[16] Therefore, the intermediates formed with $\omega(H_2O)$ = 0.2, 1.0, 2.0, and 6.0% were analyzed. Figure 5 shows the mass fraction of the intermediate product $N_2O_4(H_2O)_n$ for different $\omega(H_2O)$. As shown in Figure 5a, at $\omega(H_2O)$ = 0.2%, the intermediate product is only $N_2O_4(H_2O)$, the yield of which increases rapidly and remains stable for a long period of time with the mass fraction maintained at about 0.12%. As $\omega(H_2O)$ continues to increase, as shown in Figure 5b, a small amount of $N_2O_4(H_2O)_2$ appears, but the main intermediate product is still $N_2O_4(H_2O)$. Then, as shown in Figure 5c, the yield of $N_2O_4(H_2O)$ further increases at $\omega(H_2O)$ = 2.0% and the yield of $N_2O_4(H_2O)_2$ tends to be stabilized; N_2O_4 combines with H_2O in the local region of the system and produces $N_2O_4(H_2O)_3$, but the yield of $N_2O_4(H_2O)_3$ is unstable and low. When $\omega(H_2O)$ = 6.0%, the mass percentage of its intermediate product $N_2O_4(H_2O)_2$ increases dramatically, and although its yield exceeds that of $N_2O_4(H_2O)$, the $N_2O_4(H_2O)$ content does not change substantially with respect to that corresponding to $\omega(H_2O)$ = 2.0%; this indicates that when $\omega(H_2O)$ = 6.0%, the $N_2O_4(H_2O)$ content in the system is saturated and that some N_2O_4 would bind more H_2O. Therefore, the yield of $N_2O_4(H_2O)_2$ increases dramatically and stabilizes; at the same time, after the system reaches equilibrium, the yield of $N_2O_4(H_2O)_3$ also tends to stabilize to 1.0%.

3.3. Reaction Mechanism. The results of the previous study of this group show that the reaction of one N_2O_4 molecule with different amounts of H_2O result in complexes with different structures,[29] as shown in Figure 6. One N_2O_4 molecule combines with one H_2O molecule to form $N_2O_4(H_2O)$, which has only one stable structure, namely, IM1, as shown in Figure 6a. However, when one N_2O_4 molecule combines with two H_2O molecules, two structures are formed: two H_2O molecules located on the same side of

https://doi.org/10.1021/acsomega.3c08695
ACS Omega 2024, 9, 18893−18900

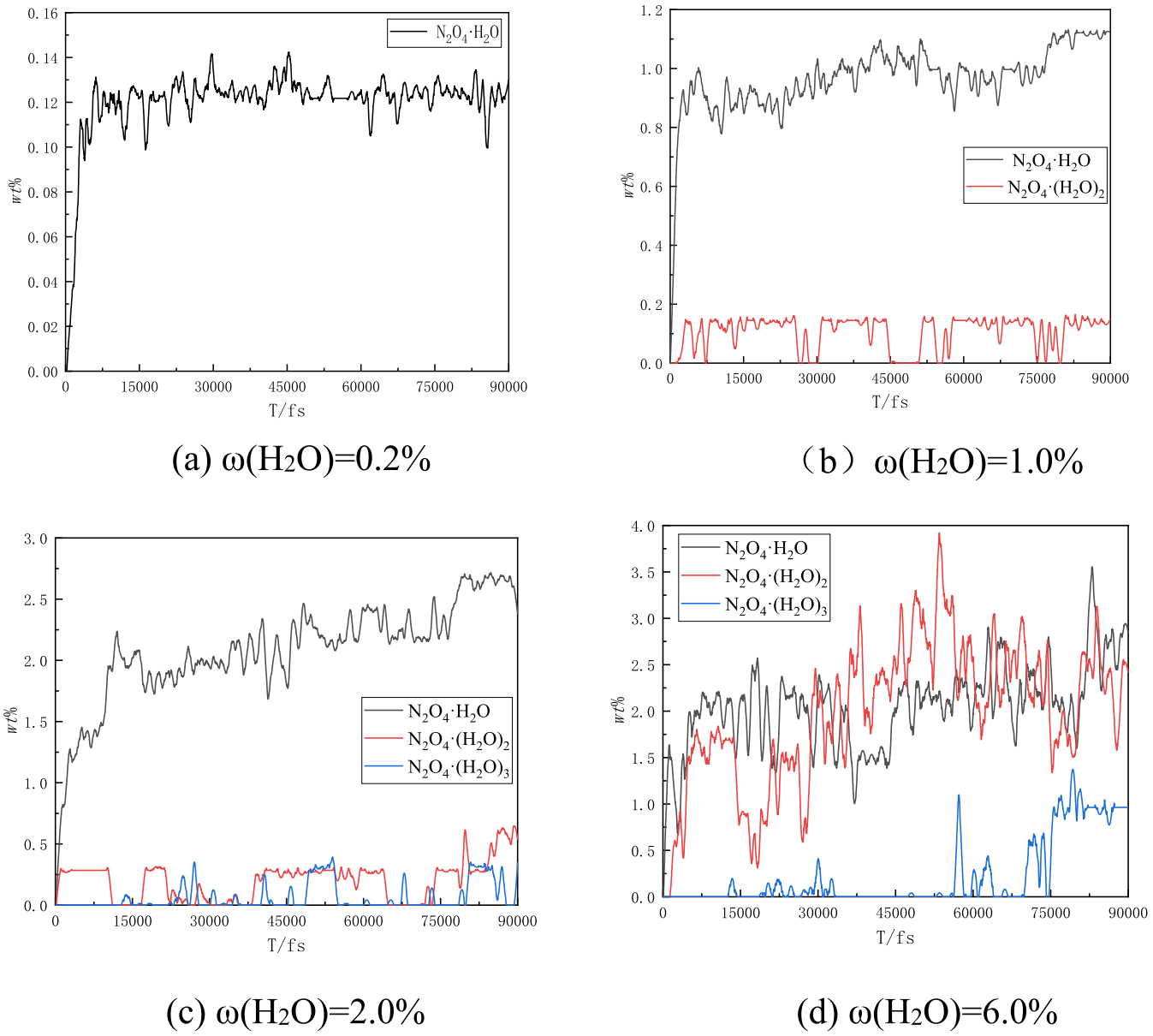

Figure 5. Mass fraction of the reaction intermediate $N_2O_4(H_2O)_n$ for the reaction of N_2O_4 with different $\omega(H_2O)$.

N_2O_4, as shown in Figure 6b, and two H_2O molecules located on both sides of N_2O_4, as shown in Figure 6c. Similarly, the combination of one N_2O_4 molecule with three H_2O molecules produces $N_2O_4(H_2O)_3$ with two structures, i.e., three H_2O molecules located on the same side of N_2O_4, as shown in Figure 6d, and two H_2O molecules on one side of N_2O_4 and one H_2O molecule on the other side, as shown in Figure 6e. When H_2O is located on the same side of N_2O_4, the number of interconnected chemical bonds is fewer and the bond length is shorter, so the reaction potential energy of IM2 and IM4 is lower and the molecular structure is more stable than those of IM3 and IM5. Thus, in summary, N_2O_4 reacts with H_2O and its intermediate products are IM1, IM2, and IM4.

After the formation of the intermediate product $N_2O_4(H_2O)_n$, there are usually two alternatives for the next reaction: the direct decomposition of $N_2O_4(H_2O)_n$ to form HNO_3 + HNO_2 and the final formation of HNO_3 + HNO_2 from $N_2O_4(H_2O)_n$ after *t*-$ONONO_2$-$(H_2O)_n$. From Sections 3.1 and 3.2, the reaction mechanisms of N_2O_4 with $\omega(H_2O)$ = 0.2, 1.0, 2.0, and 6.0% are analyzed.

$$\omega(H_2O) = 0.2\% \quad (1)$$

As can be seen from Figure 5, at $\omega(H_2O)$ = 0.2%, the only intermediate product is IM1. The reaction can proceed along both paths simultaneously because the difference between the potential energy surfaces for the two reaction paths of IM1 is small,[29] as shown in Figure 7a: (I) One $-NO_2$ in IM1 rotates along the N−N bond, which causes the shift of H_2O and the formation of *t*-$ONONO_2$−H_2O. Subsequently, the N1−O4 bond breaks, and − NO_3 and −NO combine with ionized H and −OH in H_2O to form HNO_3 and HNO_2, respectively. (II) IM1 generates HNO_3 + HNO_2 in one direct step, and the N−N bond in N_2O_4 breaks directly to form two $-NO_2$, and one combines with the detached H of H_2O to form HNO_2, while the other $-NO_2$ combines with HNO_2 remaining in H_2O to form HNO_2. NO_2 combines with the remaining −OH in H_2O to form HNO_3.

https://doi.org/10.1021/acsomega.3c08695
ACS Omega 2024, 9, 18893−18900

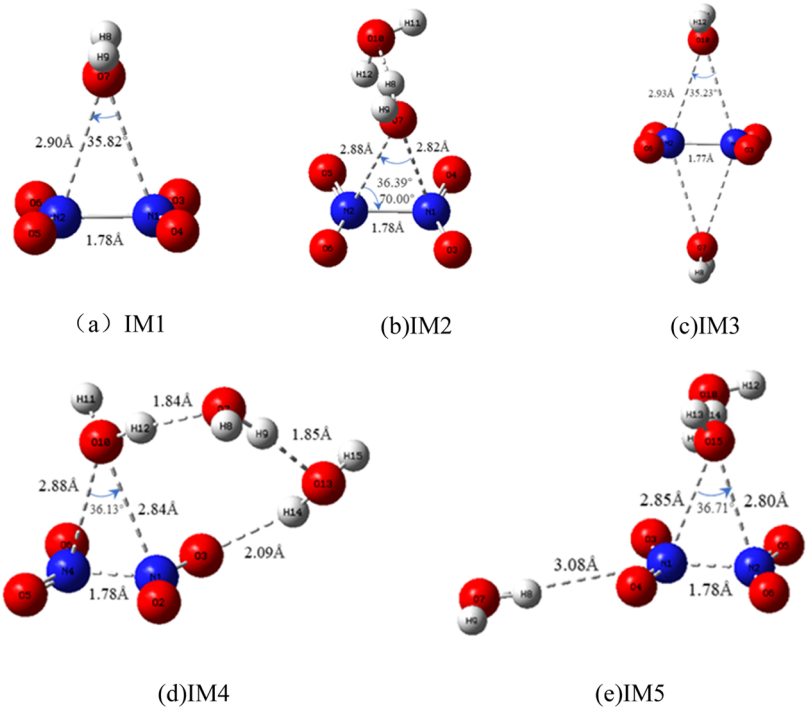

Figure 6. Structure of $N_2O_4(H_2O)_n$ (n = 1−3).

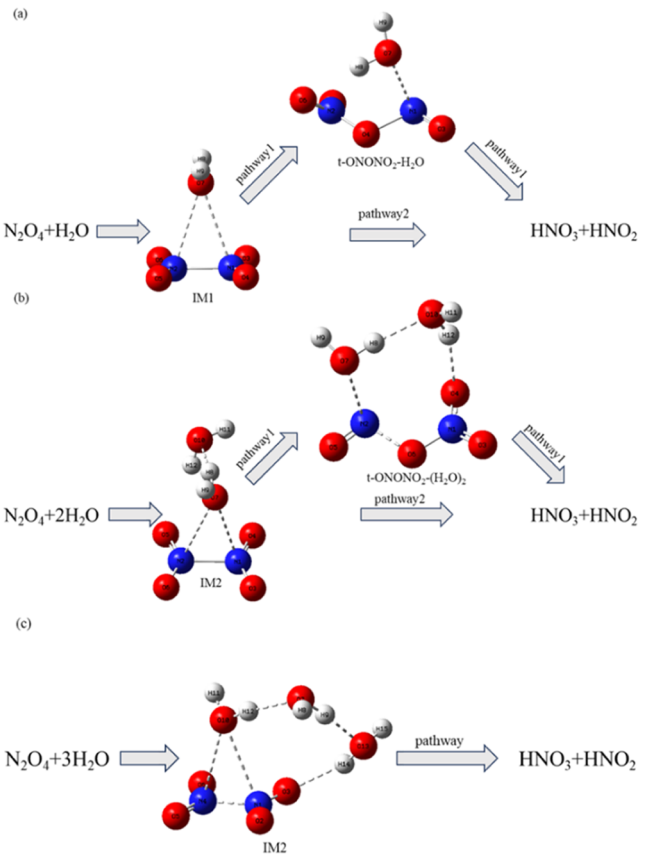

Figure 7. Reaction mechanism of N_2O_4 with H_2O.

$$\omega(H_2O) = 1.0\% \quad (2)$$

When $\omega(H_2O)$ = 1.0%, the main intermediate product of the reaction between N_2O_4 and H_2O is still IM1, and its main reaction mechanism is the same as that in Figure 7a. However, a small amount of IM2 appears, and the difference between the potential energy surfaces for the two reaction paths is small. The main reaction paths are shown in Figure 7b: (I) Both of the H_2O molecules in IM2 are involved in the reaction course, and t-$ONONO_2$-$(H_2O)_2$ is in the octameric ring structure. With the further reaction of t-$ONONO_2$-$(H_2O)_2$, proton transfer occurs in the two H_2O molecules during the process; O7 and H10 of one H_2O (O7) combine with NO to form HNO_2, and H12 in the other H_2O (O10) combines with NO_3 to form HNO_3. The remaining H8 and O10 of the two H_2O molecules recombine with H11 to form a new H_2O molecule. (II) Similar to pathway 2 of IM1 in Figure 7a, only one H_2O molecule is involved in the reaction, which ultimately produces the product directly. Further, the molecule O10 in the other H_2O interacts with H8 and O7 to form the O−H−O hydrogen bonds. According to Miller et al.,[14] t-$ONONO_2$-$(H_2O)_n$ exhibits equilibrium geometry when $n \leq 2$, and the bonding in this molecule is partly ionic but mainly covalent. Therefore, in Figure 2, the polarization curves are not regular for $\omega(H_2O) \leq 1.0\%$, and the solution system cannot form a stable current loop.

$$\omega(H_2O) = 2.0\% \quad (3)$$

When $\omega(H_2O)$ = 2.0%, the main intermediate product is still IM1, but small amounts of IM2 and IM4 are present. The reaction mechanism of IM1 and IM2 is presented in the previous section. According to Miller and previous work,[14,29] in $N_2O_4(H_2O)_n$, the two-path reaction potential of IM4 reaches 28.4 KJ·mol^{-1} at n = 3, and the reaction rate constant is higher by 2 orders of magnitude compared to that at n < 3. Further, the formation of t-$ONONO_2$-$(H_2O)_2$ is accompanied by proton transfer as the reaction proceeds. Luo et al.[24] confirmed that hydrogen bonding and a polar environment are prerequisites for intermolecular proton transfer. Moreover, the proton transfer occurring in t-$ONONO_2$ dominates the production of − OH, again supported by experimental

https://doi.org/10.1021/acsomega.3c08695
ACS Omega 2024, 9, 18893−18900

results,[30] leading to an increasingly shorter duration of existence of t-$ONONO_2$ as an increasing amount of H_2O is added. All charge transfer leaps lead to a partial reverse transfer of charge from NO_3^- to NO^+, which causes difficulty in breaking the $ON-ONO_2$ bond. Therefore, with ionic bonding being predominant in the $N_2O_4(H_2O)_3$ system, IM4 can be determined to preferentially cause the direct generation of HNO_3 and HNO_2 in one step, as shown in Figure 7c. Therefore, within the solution system, the number of ions reaches a stable value as per the polarization curve.

$$\omega(H_2O) = 6.0\% \quad (4)$$

When $\omega(H_2O)$ = 6.0%, its intermediate product species are the same as those when $\omega(H_2O)$ = 2.0%, but the dominant ones are IM1 and IM2; further, the number of IM4 is not negligible and is qualitatively higher than that at $\omega(H_2O)$ = 2.0%. The dramatic increase in the number of IM4 leads to an enhancement in the corrosion current density by about 2 orders of magnitude and the appearance of passivation regions; these results again validate the experimental results in Section 3.1. Therefore, the reaction mechanism at $\omega(H_2O)$ = 6.0% corresponds to that in Figure 7a–c.

4. CONCLUSIONS

(1) At the beginning of the reaction, the reaction product $\omega(HNO_3 + HNO_2)$ rapidly increases and then approaches dynamic equilibrium; further, $\omega(H_2O)$ increases, the potential energy of the system decreases, the rate of the reaction increases, and the rate of decomposition of HNO_2 to form HNO_3 increases.

(2) With $\omega(H_2O)$ = 0.2%, one N_2O_4 molecule combines with only one H_2O molecule to produce $N_2O_4{\cdot}H_2O$; as $\omega(H_2O)$ increases, small amounts of $N_2O_4(H_2O)_2$ and $N_2O_4(H_2O)_3$ appear as intermediates. At $\omega(H_2O)$ = 6.0%, the yield of the intermediate product $N_2O_4(H_2O)_2$ begins to exceed that of $N_2O_4H_2O$, and the $N_2O_4(H_2O)_3$ content reached 1.0%.

(3) With $\omega(H_2O)$ = 0.2 and 1.0%, the intermediate product $N_2O_4(H_2O)_n$ in the system, i.e., $N_2O_4(H_2O)_n$, reacts along two different paths when n = 1 or 2. When $\omega(H_2O) \geq 2.0\%$, the appearance of $N_2O_4(H_2O)_n$ in the system tends to produce the final product in one direct step.

AUTHOR INFORMATION

Corresponding Author

Xinlong Chang − *School of Missile Engineering, Rocket Force University of Engineering, Xi'an 710025, China*; Email: xinlongch@vip.sina.com

Authors

Yi Guo − *School of Missile Engineering, Rocket Force University of Engineering, Xi'an 710025, China*; orcid.org/0009-0006-0969-0927

Gan Tian − *School of Missile Engineering, Rocket Force University of Engineering, Xi'an 710025, China*

Zhanmei Tang − *Beijing Institute of Aerospace Testing Technology, Beijing 100074, China*

Zhiyong Huang − *School of Missile Engineering, Rocket Force University of Engineering, Xi'an 710025, China*

Dejun Liu − *School of Missile Engineering, Rocket Force University of Engineering, Xi'an 710025, China*

Xinzhi Yang − *School of Missile Engineering, Rocket Force University of Engineering, Xi'an 710025, China*

Complete contact information is available at: https://pubs.acs.org/10.1021/acsomega.3c08695

Author Contributions

Y.G.: conceptualization, investigation, methodology, and writing—original draft. G.T.: project administration and validation. X.C.: funding acquisition and writing—review and editing. Z.T.: electrochemical test. Z.H.: data curation and formal analysis. D.L.: resources and supervision. X.Y.: software and validation.

Funding

This research was funded by the National Natural Science Foundation of China (NO.52272446) and the Natural Science Foundation of Shaanxi Province (NO.2021JM-250).

Notes

The authors declare no competing financial interest.

ACKNOWLEDGMENTS

The authors are very grateful to Associate Researcher Guo Wei and engineers Peng Zheng and Jiang Manzi of the Beijing Institute of Aerospace Testing and Technology, China, for their assistance in this research.

REFERENCES

(1) Liu, D. J.; Tian, G.; Yang, Z. W.; Jin, G. F.; Zhang, W.; Wang, Y.; Wei, H. L. Stress corrosion behavior of 2195-T8 Al-Li alloy with an artificial pit exposed to a 30 vol % HNO_3 solution. *Chin. J. Aeronaut.* **2023**, *36*, 304−315.

(2) Yao, X. Q.; Wen, L.; Yu, Z. G.; Guo, W.; Huang, F. F.; Qiang, Y. J.; Jin, Y. Study on corrosion behavior and mechanism of 5A06 aluminum alloy in N_2O_4 medium. *J. Alloys Compd.* **2023**, *931*, No. 167544.

(3) Guo, Y.; Chang, X. L.; Tian, G.; Liu, D. J.; Pang, C.; Wu, W. Pre-corrosion Fatigue Performance of 2195-T8 Al-Li Alloy in N_2O_4 under Tension-Tension Load. *Rare Met. Mater. Eng.* **2022**, *51*, 3459−3465.

(4) Han, Y.; Jiang, D. D.; Zhang, J. L.; Li, W.; Gan, Z. X.; Gu, J. J. Development, applications and challenges of ReaxFF reactive force field in molecular simulations. *Front. Chem. Sci. Eng.* **2016**, *10*, 16−38.

(5) Allinger, N. L.; Yuh, Y. H.; Lii, J. H. Molecular mechanics. The MM3 force field for hydrocarbons.1. *J. Am. Chem. Soc.* **1989**, *111*, 8551−8566.

(6) Allinger, N. L.; Li, F.; Yan, L.; Tai, J. C. Molecular mechanics (MM3) calculations on conjugated hydrocarbons. *J. Comput. Chem.* **1990**, *11*, 868−895.

(7) Mayo, S. L.; Olafson, B. D.; Goddard, W. A. Dreiding: Ageneric force field for molecular simulations. *J. Phys. Chem. A* **1990**, *94*, 8897−8909.

(8) Rappe, A. K.; Casewit, C. J.; Colwell, K. S.; Goddard, W. A.; Skiff, W. M. UFF, a full periodic table force field for molecular mechanics and molecular dynamics simulations. *J. Am. Chem. Soc.* **1992**, *114*, 10024−10035.

(9) van Duin, A. C. T.; Dasgupta, S.; Lorant, F.; Goddard, W. A. Reax FF. A reactive force field for hydrocarbons. *J. Phys. Chem. A* **2001**, *105*, 9396−9409.

(10) Senftle, T. P.; Hong, S.; Islam, M. M.; Kylasa, S. B.; Zheng, Y.; Shin, Y. K.; Junkermeier, C.; Engle-Herbert, R.; Janik, M. J.; Aktulga, H. M.; Verstraelen, T.; Grama, A.; van Duin, A. C. T. The ReaxFF reactive force-field: development, applications and future directions. *npj Comput. Mater.* **2016**, *2*, No. 15011.

(11) Zhao, J. S.; Huang, Z. Y.; Jin, G. F.; Gao, M. N.; Zhu, H. X. Reactive molecular dynamics calculation and lgnition delay test of the mixture of an additive and 2-N, N-dimethylethanamine with dinitrogen tetroxide. *ACS Omega* **2022**, *7*, 14527−14534.

(12) Liu, Y.; Zybin, S. V.; Guo, J. Q.; van Duin, A. C. T.; Goddard, W. A. Reactive dynamics study of hypergolic bipropellants: monomethylhydrazine and dinitrogen tetroxide. *J. Phys. Chem. B* **2012**, *116*, 14136−14145.
(13) Liu, W. G.; Goddard, W. A. First-Principles Study of the Role of Interconversion Between NO_2, N_2O_4, *cis*-ONO-NO_2, and *trans*-ONO-NO_2 in Chemical Processes. *J. Am. Chem. Soc.* **2012**, *134*, 12970−12978.
(14) Miller, Y.; Finlayson-Pitts, B. J.; Gerber, R. B. Ionization of N_2O_4 in Contact with Water: Mechanism, Time Scales and Atmospheric Implications. *J. Am. Chem. Soc.* **2009**, *131*, 12180−12185.
(15) Pimentel, A. S.; Lima, F. C. A.; da Silva, A. B. F. The isomerization of dinitrogen tetroxide: O_2N-NO_2 → ONO-NO_2. *J. Phys. Chem. A* **2007**, *111*, 2913−2920.
(16) de Jesus Medeiros, D.; Pimentel, A. S. New Insights in the Atmospheric HONO Formation: New Pathways for N_2O_4 Isomerization and NO_2 Dimerization in the Presence of Water. *J. Phys. Chem. A* **2011**, *115*, 6357−6365.
(17) Zakharov, I. I. Quantum-chemical modeling of the mechanism for formation of HNO_3 from NO_2 and water. *Theor. Exp. Chem.* **2012**, *48*, 233−239.
(18) Zhu, R. S.; Lai, K. Y.; Lin, M. C. Ab Initio Chemical Kinetics for the Hydrolysis of N_2O_4 Isomers in the Gas Phase. *J. Phys. Chem. A* **2012**, *116*, 4466−4472.
(19) Putikam, R.; Lin, M. C. A novel mechanism for the isomerization of N_2O_4 and its implication for the reaction with H_2O and acid rain formation. *Int. J. Quantum Chem.* **2018**, *118*, 25560−25569.
(20) Finlayson-Pitts, B. J.; Wingen, L. M.; Sumner, A. L.; Syomin, D.; Ramazan, K. A. The heterogeneous hydrolysis of NO_2 in laboratory systems and in outdoor and indoor atmospheres: An integrated mechanism. *Phys. Chem. Chem. Phys.* **2003**, *5*, 223.
(21) Martins-Costa, M. T. C.; Anglada, J. M.; Francisco, J. S.; Ruiz-Lopez, M. F. The Aqueous Surface as an Efficient Transient Stop for the Reactivity of Gaseous NO_2 in Liquid Water. *J. Am. Chem. Soc.* **2020**, *142*, 20937−20941.
(22) Menezes, F.; Popowicz, G. M. Acid Rain and Flue Gas: Quantum Chemical Hydrolysis of NO_2. *Phys. Chem.* **2022**, *23*, 395.
(23) Miller, Y.; Gerber, R. B. Dynamics of proton recombination with NO_3^- anion in water clusters. *Phys. Chem. Chem. Phys.* **2008**, *10*, 1091−1093.
(24) Luo, G. F.; Chen, X. B. Ground-State Intermolecular Proton Transfer of N_2O_4 and H_2O: An Important Source of Atmospheric Hydroxyl Radical? *J. Phys. Chem. Lett.* **2012**, *3*, 1147−1153.
(25) Brown, C. T. *Feasibility Studies of an Electrochemical Test Method for Nitrogen Tetroxide Compatibility Testing (Task II, Report)*, AFRPL-TR-78−72, 1978.
(26) Biovia, D. S. *Materials Studio*; Dasault Systemes, San Diego, 2017.
(27) Plimpton, S. Fast parallel algorithms for short-range molecular dynamics. *J. Comput. Phys.* **1995**, *117*, 1−19.
(28) Rahaman, O.; van Duin, A. C. T.; Goddard, W. A.; Doren, D. J. Development of a ReaxFF Reactive Force Field for Glycine and Application to Solvent Effect and Tautomerization. *J. Phys. Chem. B* **2011**, *115*, 249−261.
(29) Guo, Y.; Huang, Z. Y.; Tian, G.; Wu, W.; Lin, J.; Chang, X. L. Isomerization and reaction process of $N_2O_4(H_2O)_n$. *RSC Adv.* **2023**, *13*, 12469−12475.
(30) Kinugawa, T.; Enami, S.; Yabushita, A.; Kawasaki, M.; Hoffmann, M. R.; Colussi, A. J. Conversion of gaseous nitrogen dioxide to nitrate and nitrite on aqueous surfactants. *Phys. Chem. Chem. Phys.* **2011**, *13*, 5144−5149.

https://doi.org/10.1021/acsomega.3c08695
ACS Omega 2024, 9, 18893−18900